Electronic noise analysis of a 127-micron pixel TFT/photodiode array

Richard L. Weisfield and N. Robert Bennett

dpiX, LLC, Palo Alto, CA, 94304

ABSTRACT

In this paper we examine origins of electronic noise in a 127-micron pixel thin film transistor (TFT)/photodiode image sensor array. The imaging array is a 1536 data line by 1920 gate line amorphous Silicon (a-Si) sensor array connected to low noise charge amplifiers and 14-bit electronics. We measure the contributions of A/D converters, charge amplifiers, data-line resistance and capacitance, and pixel switching to the overall electronic noise of 1040 e^- per pixel. Noise power spectra are evaluated for each dark offset image. When suitably filtered linear power supplies are used for supplying gate and bias voltages to the array, the noise power spectra are identical in the x and y directions, i.e., row correlated noise is negligible. Noise measurements taken under different band-pass conditions correlate well with data-line resistance generated Johnson noise. No variations in noise along the data lines and a slight reduction in noise along the gate lines suggest only small transmission line effects. Pixel noise was measured as a function of frame time, yielding a component of noise due to TFT switching and a frame time dependent component modeled as pixel leakage current shot noise. It was found that this shot noise current was three times higher than leakage currents derived from dark offset difference images.

Keywords: a-Si, TFT, photodiode, pixel, digital imaging, electronic noise, noise power spectrum, sensor array.

1. INTRODUCTION

Several authors[1, 2, 3] have reported previously on the total amounts of electronic noise in their imaging systems. DQE at low x-ray exposures in digital image sensors is ultimately limited by electronic noise. Various components of electronic noise, both correlated and uncorrelated, can influence design considerations for the image sensor. The purpose of this paper is to present experimental results evaluating various contributions to electronic noise from a particular amorphous silicon image sensor array and relate it to design characteristics of the array and imaging electronics. For this purpose, we have utilized a highly programmable imaging system utilizing a 127-micron pixel TFT/photodiode image sensor array with an active area of 195×244 mm^2. The imaging array has 1536 data lines and 1920 gate lines, and is connected to low noise charge amplifiers and 14-bit Analog to Digital conversion electronics. Under optimized conditions of operation, the noise per pixel is approximately 1040 e^-.

Our basic approach is to measure noise power spectra of dark images under different experimental conditions. Noise power spectra are obtained by evaluating the noise power of dark images in both the x and y directions. A typical example is shown in Figure 1. The X NPS spectrum shows variations from data line to data line, and increases at very low spatial frequencies due to fixed pattern noise. The Y NPS spectrum shows variations from gate line to gate line, and can show noise in excess of that observed in the X NPS spectrum due to row correlated noise coupled in from noise on the voltages connected to the array. By suitable filtering of the power supplies connected to the array, row correlated noise becomes relatively small, so the average noise power becomes flat and uniform in both x and y directions for all spatial frequencies below the Nyquist limit, which for this array is 3.94 mm^{-1}. In general, we use the average noise power in the x direction (data line varying) as the measure of noise power.

The average noise power multiplied by the Nyquist frequency is equal to the variance of the noise in the image, neglecting any fixed pattern noise or row correlated noise artifacts. Since various contributions of noise add as the sums of their squares, the average noise power for each component of noise is the metric we use to show the stack-up of noise contributors. We also find that the image noise is stationary, in the sense that RMS variations in dark images from frame to frame equal the variance within a given image times $\sqrt{2}$. The noise we will report here is the average noise power and equivalent charge noise expressed in units of electrons (e^-). This represents the standard deviation of the electronic signal within a dark image.

One of the key things we intend to determine is the separate contributions to dark noise from baseline noise of the ADC electronics, the noise from the charge amplifiers, the Johnson noise generated by the resistance of the data lines, and pixel noise. In a previous report[3] on a larger 30×40 cm^2 imager with identical 127-micron pixels, we obtained 1600 e^- of noise

per pixel. It will be shown that the excess noise generated in this larger array compared to the 1040 e^- of noise obtained in the array evaluated in this paper can be completely attributed to the extra line noise associated with the higher data-line resistance and capacitance of the array. These results are presented in Section 3.

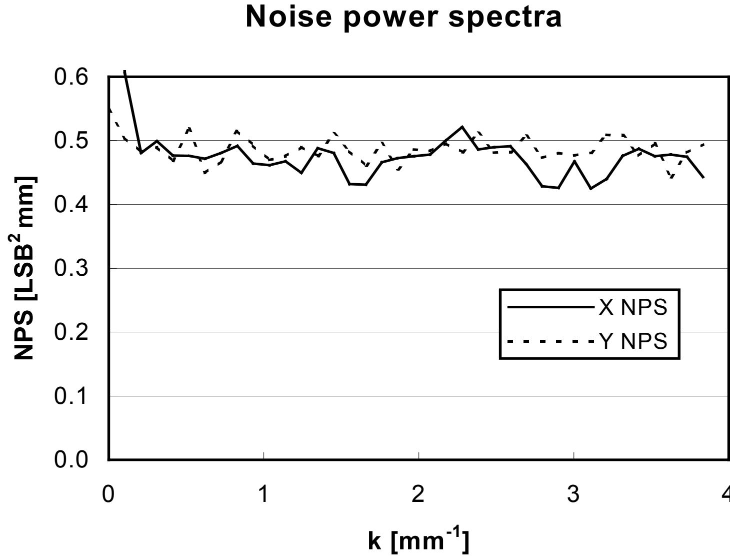

Figure 1. Noise power spectra in the x and y directions. X NPS varies with data line and Y NPS varies with gate line.

A second point of interest is the spatial uniformity of electronic noise in a large area array. It has been reported previously[4] that one should expect spatially varying effects in both x and y directions due to transmission line effects of the gate and data lines. We have examined the noise characteristics vs. position in the image and will report on these results in Section 4.

Another item that we would like to better understand is the origins of pixel noise. The dominant component of pixel noise comes from the interaction of the TFT switch with the photodiode capacitance. This so-called kTC noise equals:

$$\sigma_{kTC} = \sqrt{2kTC_{PD} / q} .$$

Not included in the above equation, are additional noise components due to charge trapping in the TFT and shot noise associated with the leakage currents of the TFT and photodiode. These noise sources are addressed in Section 5.

2. EXPERIMENTAL METHODOLOGY

A block diagram of the imaging system is shown in Figure 2. The system consists of the sensor array, with gate driver chips connected to blocks of gate lines and custom readout chips connected to blocks of data lines, and system electronics. The sensor array consists of a matrix of a-Si TFTs and *nip* photodiodes, whose characteristics are described elsewhere[5]. The peripheral integrated circuits are connected to the glass using tape automated bonding (TAB). The readout chips contain low noise charge amplifiers, double correlated sampling circuits with programmable filtering, and analog multiplexers to stream out the image data at video rates. The image signals are amplified and converted to digital images with 14-bit analog to digital converters (ADCs). For the purposes of this study, the ADC electronics and charge amplifiers are operated in a high gain mode, so that each least significant bit (LSB) corresponds to an equivalent charge of 145 e^-. The readout ICs can be operated with different degrees of internal filtering, achieved by switching in different resistors in series with each amplifier's sample and hold circuit.

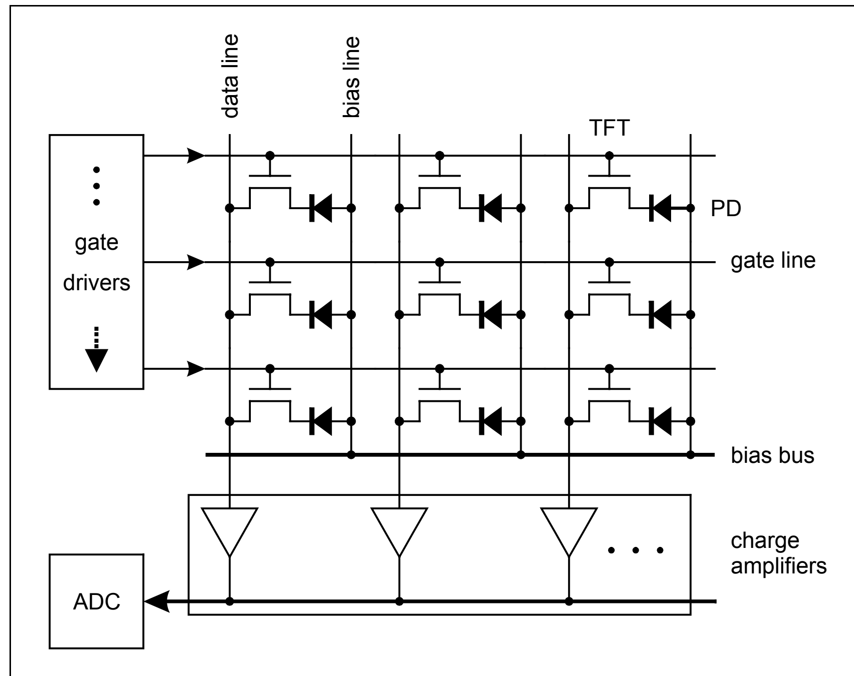

Figure 2. Imaging system block diagram featuring a matrix of TFT/PD pixels.

To reduce noise as much as possible, the readout sequence employs double-correlated sampling. The circuit for an individual input channel connected to an arbitrary pixel is shown in Figure 3.

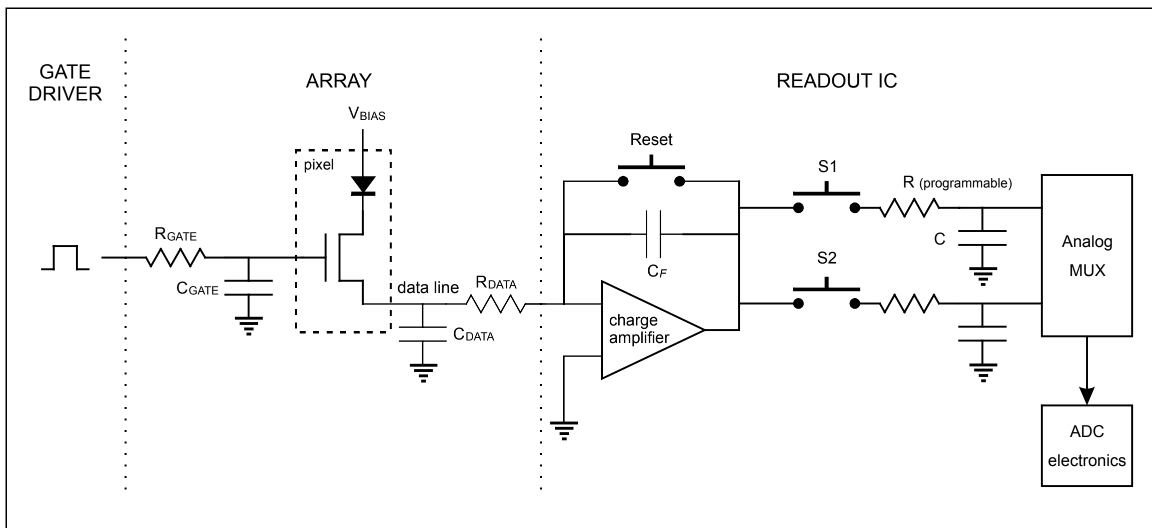

Figure 3. Circuit for double-correlated sampling read-out sequence.

The readout sequence is as follows: The data lines are clamped to virtual ground except during the period of time when the reset switch is turned off. The charge signal on each data line is sampled before and after a gate pulse is applied to each TFT through two sample and hold circuits per charge amplifier, and the resulting difference becomes the signal measured. During the two sampling periods S1 and S2, a pass transistor is connected between the output of the charge amplifier and a storage capacitor through a user selectable resistor. The RC time constant was varied between 1 μs and 4 μs, with a default time constant of 3 μs used under normal modes of operation. Sampling times of 12 μs were chosen so as to be long compared to the time constants used in this experiment. A 10 μs gate pulse was used, which has been found to transfer more than 99% of the charge from frame to frame. A timing diagram for the double-correlated sampling is illustrated in Figure 4.

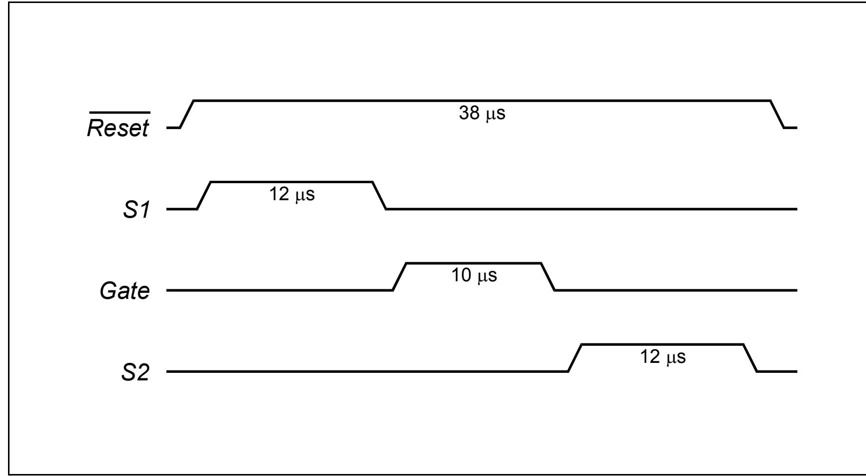

Figure 4. Timing of double-correlated sampling read-out.

3. LINE NOISE CONTRIBUTORS

In this section we evaluate the various contributions of noise of the ADC electronics, the noise from the charge amplifiers, the Johnson noise generated by the resistance of the data lines, and pixel noise.

A series of dark images were measured under different experimental conditions:
First, we took an image with only the ADC electronics contributing a signal. The noise level in high gain mode was 2 LSB.
Second, we took an image with the charge amplifiers connected to the ADC electronics but disconnected from the array. This image contains the noise power of the ADC electronics added to the noise power of the charge amplifiers. By subtracting out the noise power of the ADC electronics we can obtain the noise of the charge amplifiers when they are not loaded by array capacitance, which turns out to be approximately 400 e^-. We measured this noise for different levels of internal filtering, and found that the charge amplifier noise was rather insensitive to bandwidth limiting conditions.
Third, we connected the array to the charge amplifiers and obtained images with the gates kept off. These images contain the noise of the ADC electronics, the noise of the charge amplifiers, and data line noise. Data line noise is generated by resistive Johnson noise on each data line and noise associated with the capacitance at the input to each charge amplifier. We measured the line noise for different degrees of filtering. Typical line noise with 3 μs of filtering was 780 e^-. We fitted the experimental results to a frequency dependent component associated with the Johnson noise generated by the data line resistance and capacitance, and a separate component of noise coming directly from the charge amplifiers. We used the following formula for Johnson noise:

$$\sigma_J = \sqrt{4kTR_{data}\Delta f} \cdot C_{data} ,$$

where R_{data} and C_{data} are the array's data line resistance (1300 Ω) and capacitance (60 pF). The bandwidth $\Delta f = 1/(4\tau_{RC})$, ranging from 63 to 220 kHz for different RC settings, was determined from an analysis of frequency response of a double correlated sampler with an internal low-pass RC filter.

We found that the charge amplifier noise increases to 600 e^- when connected to the 60 pF of data line capacitance, and that the room temperature Johnson noise with 83 kHz of filtering is about 500 e^-.
Finally, we introduced normal gate pulsing and measured the noise power of dark images. These images have an added component of noise associated with the readout of each pixel. This noise turned out to be about 630 e^- at typical frame rates of about 3 frames per second. How this pixel noise changes with frame time is reported in Section 5.

The main results of the experiment are shown in Figure 5, where we plot the various components of noise power (in units of LSB^2·mm) against the internal time constant of the charge amplifier.

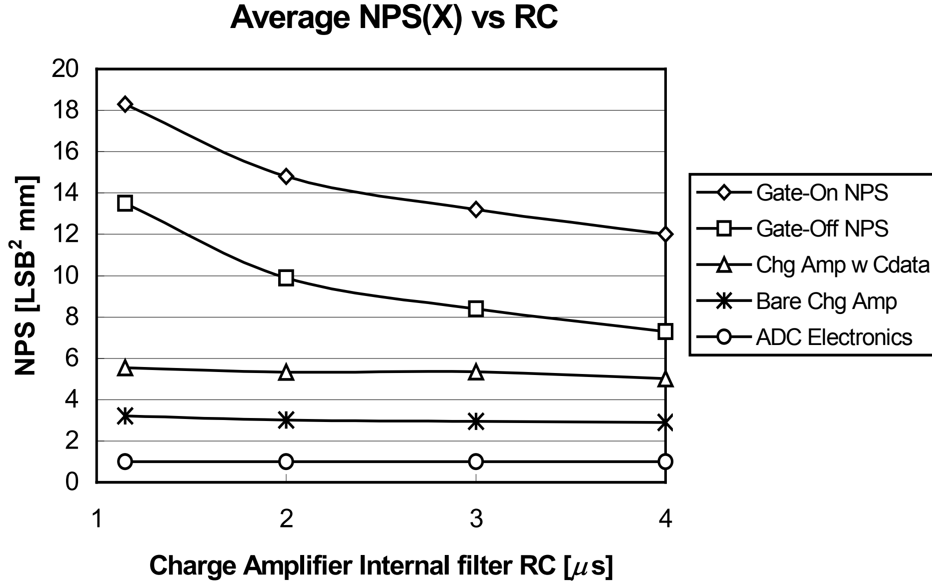

Figure 5. Noise power vs. internal RC time constant of charge amplifier.

The bottom curve (ADC Electronics) is the baseline noise associated with the electronics associated with the voltage amplifiers and A/D converters. This amounts to an equivalent noise of 2 LSB, or equivalently, 290 e^-.
The second curve (Bare Chg Amp) is the noise of the charge amplifiers using the same electronics but not connected to an array. The noise of the charge amplifier by itself is about 400 e^-, or 555 e^- including the rest of the system electronic noise, and is rather insensitive to the sampling bandwidth.
The curve for Gate-Off NPS represents the noise of the image measured when the gates are turned off. It includes the noise associated with the charge amplifiers connected to the data lines, as well as the resistive Johnson noise associated with the data lines. The Gate-Off NPS was measured for four separate RC time constants, and it is quite apparent that the noise is sensitive to the RC time constant selected. Using measured data-line parameters, we calculate the associated room temperature Johnson noise for each bandwidth in Table 1.

Table 1. Johnson noise [e^-] as a function of bandwidth.

Time Constant [μs]	1.15	2	3	4
Calculated Johnson Noise [e^-]	811	611	502	435

If we subtract off these calculated contributions to the Gate-Off NPS, we obtain the third line in the noise plot, namely the amplifier noise with array connected to readout chips. This line is quite flat with bandwidth, and represents the noise of the charge amplifier connected to a pure data-line capacitance without added electrical resistance. We thus infer a total charge amplifier noise of 600 e^- when connected to a data-line capacitance of 60 pF. We can use this to estimate a linear relationship between charge amplifier noise and data-line capacitance as follows:

$$\sigma_{AMP} = 400\ e^- + (3.3\ e^- / \text{pF}) \times C_{data}\ [\text{pF}].$$

The top curve of the noise plot (Gate On NPS) is obtained with the gate turned on. Note that there is a constant offset in noise power between the "Gate-Off" and "Gate-On" curves. This added noise is associated with reading out each individual pixel and amounts to noise of from 630 e^- to 650 e^-. Each pixel has a photodiode with a capacitance C_{PD} of 0.7 pF. The largest contribution to the noise comes from the switching noise σ_{kTC} = 500 e^-, when each photodiode is sampled and then reset to ground. Other noise contributions arise from TFT trapping noise and photodiode shot noise. These additional noise measurements are discussed in Section 5.

The overall noise under normal operation for this array is 1040 e^-, consisting of 290 e^- from the ADC electronics, 600 e^- from the charge amplifier, 500 e^- of resistive Johnson noise, and 630 e^- of pixel noise. When we consider the 30 × 40 cm^2 array discussed previously[3], we reported 1600 e^- of noise in a dark image. This larger array has a data-line resistance of 2000 Ω and capacitance of 100 pF, using the same charge amplifier as in this study, but with a time constant of 2 μs. The frame time was 3.2 seconds, so the pixel noise was slightly larger, namely 650 e^-. Based on our understanding of the smaller array, we can calculate the performance of the larger array with these characteristics. The charge amplifier noise, σ_{AMP}, is 735 e^-, the resistive Johnson noise, σ_J , is 1280 e^-, and the pixel noise is 650 e^-. These contribute to an overall noise of 1610 e^-, which is consistent with what we reported previously[3]. It is clear that data-line resistive Johnson noise becomes the dominant noise component for high values of data-line resistance and capacitance. Minimizing these noise components in large area arrays is an important design consideration.

4. TRANSMISSION LINE EFFECTS

Image noise was evaluated as a function of position in the image. No variation was observed from top to bottom (the y direction) in either component of noise power. The vertical direction of the array is the direction in which the data lines run. The lack of variation in noise along the data lines implies that there are no significant transmission line effects along the data lines, contrary to what was predicted by Huang *et al* [4]. In the array described in that paper, the data-line resistance and capacitance was much higher than in the array they were analyzing. Because the resistance and capacitance of the data lines here are much smaller, the data line can be treated as a lumped circuit, since its time constant of 78 ns is short compared to the other time constants in the system.

On the other hand, we did find transmission line effects when we measured the noise at different positions along a gate line (the x-direction). These results are shown in Figure 6.

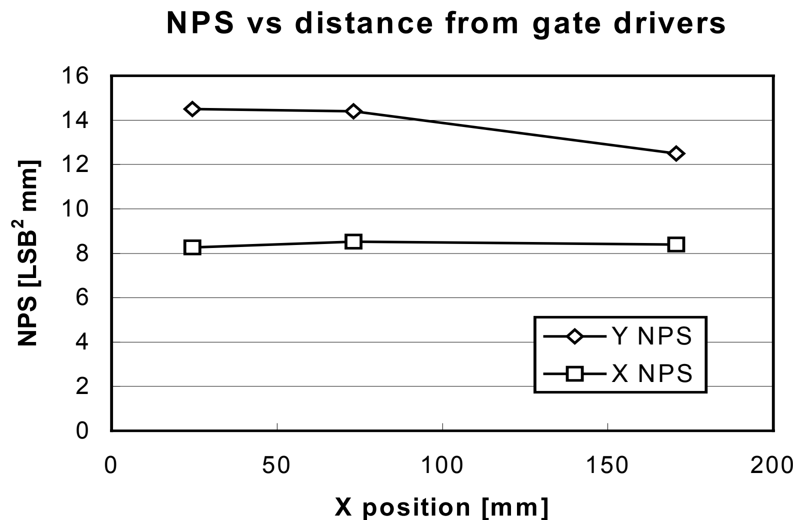

Figure 6. X and Y average noise power as a function of distance from the gate drivers.

The X NPS, which measures the noise varying between adjacent data lines, did not appear to be sensitive to position in the image. This is in keeping with the low resistance of the data lines. However, the Y NPS, which measures the noise between adjacent gate lines, decreases as one traverses from the left end of the image to the right. This clearly demonstrates a transmission line effect along a gate line. The left hand side of the imager has gate drivers connected to it, and gate pulses transit across the gate lines from left to right. It appears that the gate drivers induce excess line noise, which damps out as the gate pulse traverses along each gate line. Because the gate-line resistance and capacitance are 12 kΩ and 70 pF, respectively, the RC delay is 0.84 μs, which is a significant time constant compared to the other time constants in the pixel readout timing. Probably, the excess noise is caused by gate to data or gate to pixel coupling caused by the sharp rise and fall times of the gate pulses (< 100 ns). Near the undriven end of the gate lines, the gate pulses are more rounded due to the RC delay,

dampening the effect of this coupling noise. For the purposes of this paper, noise was measured in the center of the image, where any influence from the proximity to the gate drivers is less severe.

One result of this observation is that dark level correction can have an unexpected spatial dependence across an image. As has been discussed in an earlier paper[6], the purpose of dark level correction is to minimize row-correlated noise. The correction is done by subtracting the average signal from a set of dark pixels at one end of the image in each row, from all the other pixel values in a given row. The assumption is that the same row correlated noise is injected into every pixel in a given row. The fact that Y NPS can vary from one end of the image to the other implies that if the dark zone is taken at the driven end of each gate line, the noise will be over-subtracted at the undriven side of the image, and *visa versa*. This effect should be considered when applying dark level correction in a large area image.

5. PIXEL NOISE

In this section we examine sources of pixel level noise more carefully. The pixel noise of 630 e^- is somewhat larger than the estimated 500 e^- of kTC noise associated with the pixel capacitance. We consider two additional contributors to the pixel noise: noise coming from charge trapped in the TFT shortly after it is shut off and shot noise associated with the leakage currents of the TFT and photodiode in each pixel. The charge trapped in the TFT should be a property of the size of the TFT and the density of deep level defects in the a-Si channel layer. We estimate that this would produce about 130,000 e^- of trapped charged for a gate length $L = 8\ \mu$m, a gate width $W = 16\ \mu$m, and a deep level density of $N_T = 1 \times 10^{11}$cm^2. The noise associated with this trapped charge is:

$$\sigma_T = \sqrt{WLN_T} = \sqrt{130000}e^- = 360e^- .$$

Shot noise σ_S depends on the integrated amount of current leaking onto the pixel over a frame time τ_F. We can determine the leakage current as a function of time by measuring the average dark offset of the image as a function of frame time. This measurement is shown in Figure 7. The slope of the offset signal is proportional to the leakage current, shown in Figure 8.

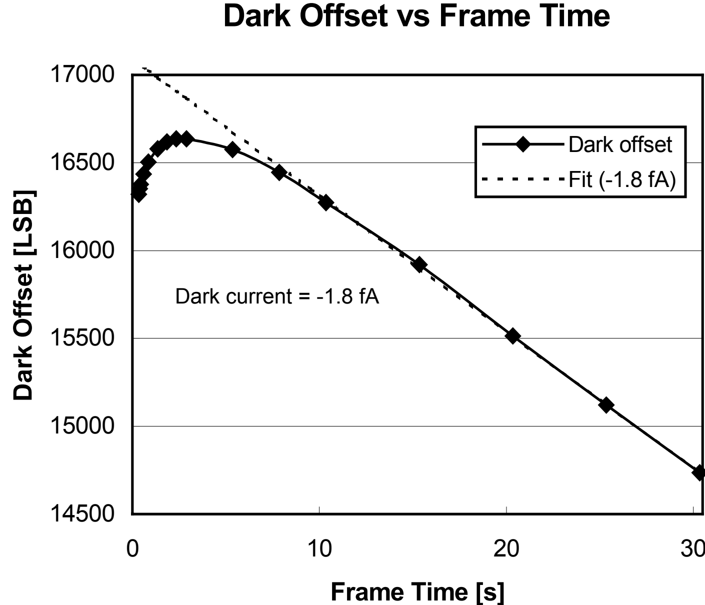

Figure 7. Dark offset vs. frame time, plus a linear fit using a leakage current of –1.8 fA.

For frame times longer than about 5 seconds, the offset signal decreases linearly with time, which we attribute to the dark current of the photodiode. We fit the long time behavior to a constant current of –1.8 fA. We attribute this long time behavior to the steady state dark current of the photodiode. For frame times shorter than about 3 seconds, the leakage current is positive and decreases very rapidly with time. This rapidly decaying positive current corresponds to the decay of the TFT

leakage current after it is turned off. When we subtract off the dark current from the total leakage current, we obtain a measure of the decaying TFT off current separately, which is also plotted vs. frame time in Figure 8.

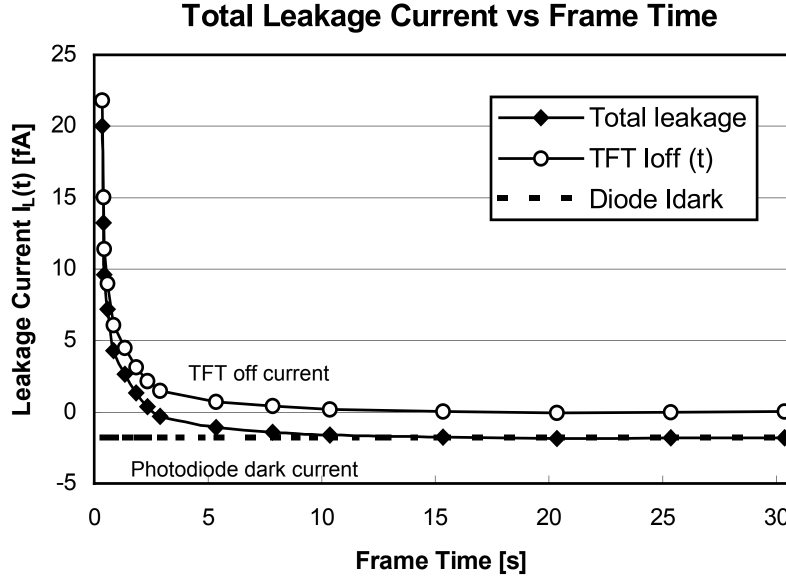

Figure 8. Leakage current as a function of frame time. Leakage current beyond 10 seconds is a constant –1.8 fA. Short time leakage is dominated by time dependent off current of the TFT $I_{off}(t)$.

The leakage charge is defined by the following:

$$Q_L = \int I_L(t)dt / q \,,$$

where I_L is the pixel leakage current (the sum of decaying TFT off current, $I_{off}(t)$, at short times and photodiode dark current, I_D, for long frame times), integrated over the frame time τ_F. We determine the shot noise, σ_S, as the sum of the contributions from TFT and diode leakage:

$$\sigma_S = \sqrt{\frac{\int I_{off}(t)dt + |I_D \tau_F|}{q}} \,.$$

For a typical dark current I_D = 2 fA and 1 s frame time, the leakage charge Q_L = 2 fC, and σ_S = 110 e^-. Combining these three sources of noise, σ_{kTC} = 500 e^-, σ_T = 400 e^-, and σ_S = 110 e^-, we obtain an overall pixel noise of 625 e^-, which is very close to the 630 e^- observed.

To further check this model, we have taken noise measurements as a function of frame times ranging from 0.35 s to 30 s. In Figure 9, we show the average noise power measured vs. frame time. We also show the average noise power for just the line noise component of the noise power (8.2 LSB^2·mm), obtained by analyzing images where the gates are not pulsed. On top of this noise we show an extra noise contribution of 3.0 LSB^2·mm for the estimated 500 e^- of kTC noise.

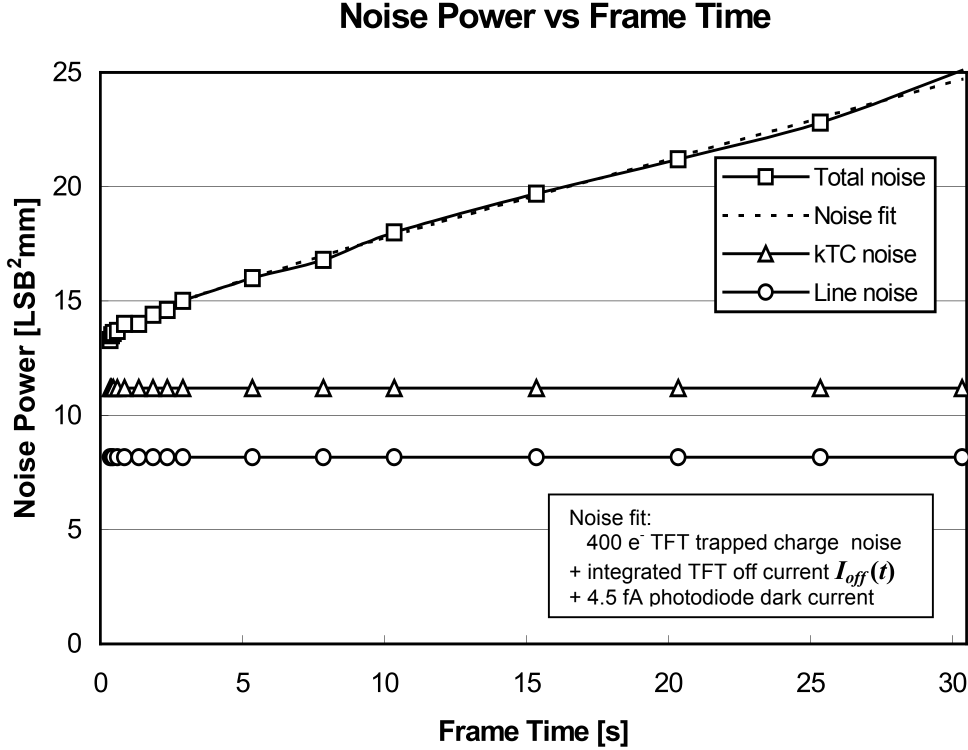

Figure 9. Total noise power vs. frame time, compared to line noise, *kT*C noise, and a fit with a TFT trapping noise of 400 e^- plus a frame-time dependent shot noise, assuming $I_{off}(t)$ as in Figure 8, and 4.5 fA of photodiode dark current.

We fit the excess pixel noise power to a curve in which the y-intercept determines the TFT trapping noise (400 e^-) and the slope of the curve determines the shot noise. At short frame times, the shot noise increases more rapidly as the off current noise of the TFT is integrated. For long frame times, the shot noise power increases linearly with time. The 400 e^- of TFT trapping noise is comparable with our previous estimate of 360 e^- using a reasonable density of a-Si defects of 1×10^{11} cm^{-2}. However, the pixel leakage current we need to fit to the excess shot noise is 4.5 fA, approximately 2.5 times larger than what we obtain by measuring the dark signal itself as a function of frame time.

At this point, it is not clear why the long-term shot noise increases at a faster rate than that predicted by the direct measurement of leakage current. This discrepancy may possibly be due to an additional component of time dependent noise beyond that of photodiode dark current that has not yet been identified. Additionally, the amount of noise associated with TFT trapped charge cannot be fully distinguished from the decay of TFT off current. Shorter time measurements of pixel noise and TFT leakage current would help to resolve this point.

6. SUMMARY

Electronic noise contributions have been evaluated in dark images of an a-Si TFT/photodiode imaging array. Spatially varying noise information has been related to transmission line effects along resistive gate lines. Pixel noise has been evaluated as a function of frame time to separate TFT trapping noise from leakage current induced shot noise. A discrepancy between shot-noise derived leakage and direct measurements of leakage current has been identified, and remains to be better understood.

The various noise components presented thus far are summarized in Table 2, for room temperature measurements of noise and an RC time constant of 3 μs. Total dark noise under these conditions is approximately 1040 e^- per pixel. By reducing the bandwidth, Johnson noise can be further suppressed, and noise less than 1000 e^- can be achieved.

Table 2. Individual sources of electronic noise

Noise type	Symbol	Form of equation	Source of noise	Noise $[e^-]$
ADC noise	σ_{ADC}	*2 LSBs*	ADCs amplifier electronics	290
Resistive Johnson noise	σ_J	$\sqrt{4kTR_{data}\Delta f} \cdot C_{data}$	data-line resistance data-line capacitance	500
Charge amplifier noise	σ_{AMP}	400 e^- + (3.3 e^- / pF) × C_{data} [pF].	charge amplifier design data-line capacitance	600
kTC switching noise	σ_{kTC}	$\sqrt{2kTC_{PD} / q}$	pixel capacitance	500
TFT trapping noise	σ_T	$\sqrt{WLN_T}$	TFT width and length a-Si trap density	400
Shot noise	σ_S	$\sqrt{(\int I_{off}(t)dt + \lvert I_D \tau_F \rvert) / q}$	leakage current frame time	110

These noise sources are further categorized as cumulative sources in Table 3.

Table 3. Cumulative noise sources

Noise type	Symbol	Form of equation	Noise $[e^-]$
Line noise	σ_{line}	$\sqrt{\sigma_J{}^2 + \sigma_{AMP}{}^2}$	780
Pixel noise	σ_{pixel}	$\sqrt{\sigma_{kTC}{}^2 + \sigma_T{}^2 + \sigma_S{}^2}$	630
Total noise	σ_{total}	$\sqrt{\sigma_{ADC}{}^2 + \sigma_{line}{}^2 + \sigma_{pixel}{}^2}$	1040

7. ACKNOWLEDGEMENTS

The authors would like to acknowledge the contributions of Koorosh Aflatooni, Paul Encoyand, Trinhi Lieu, Troy Rodgers, Roger Schneider, and Steve Valizadeh to the design of the imager used in this evaluation.

8. REFERENCES

1. T. Ducourant, M. Michel, G. Vieux, T. Peppler, J. C. Trochet, R. F. Schulz, R. Bastiaens, F. Busse, “Optimization of key building blocks for a large area radiographic and fluoroscopic dynamic digital x-ray detector based on a-Si:H/CsI:Tl flat panel technology,” *Proceedings of the SPIE* 3977, pp. 14-25, 2000.
2. T. J. C. Bruijns, T. Aadriaansz, A. R. Cowen, A. G. Davies, S. M. Kengyelics, K. Kiani, H. Kroon, H. Luijendijk, “Simulation of the image quality of an a-Si flat panel x-ray detector system in low dose fluoroscopic applications,” *Proceedings of the SPIE* 3977, pp. 117-127, 2000.
3. R. L. Weisfield, M. Hartney, R. Schneider, K. Aflatooni, R. Lujan, “High performance amorphous silicon image sensor for x-ray diagnostic medical imaging applications,” *Proceedings of the SPIE* 3659, pp. 76-89, 1999.
4. Z. S. Huang, G. De Crescenzo, J. A. Rowlands, “Signal and noise analysis using transmission line model for larger-area flat-panel x-ray imaging sensors,” *Proceedings of the SPIE* 3659, pp. 307-317, 1999.
5. R. L. Weisfield, Large-Area Amorphous Silicon TFT-Based X-Ray Image Sensors for Medical Imaging and Non Destructive Testing, *Electrochemical Society Proceedings of the Fourth Symposium on Thin Film Transistor Technologies*, 98-22, pp. 369-380, 1998.
6. R. L. Weisfield, M. A. Hartney, R. A. Street, R. B. Apte, “New amorphous-silicon image sensor for x-ray diagnostic medical imaging applications,” *Proceedings of the SPIE* 3336, pp. 444-452, 1998.